The International Journal Of Engineering And Science (IJES)
||Volume||2 ||Issue|| 7 ||Pages|| 60-77||2013||
ISSN(e): 2319 – 1813 ISSN(p): 2319 – 1805

53 nm Wavelength Tunability due to a Curvature of S-Bend in 1×2 Optical Power Splitter

Ajay Kumar[1], S. K. Raghuwanshi[2], and Santosh Kumar[3]
Photonics Lab, Department of Electronics Engineering,Indian School of Mines, Dhanbad, India

----------***ABSTRACT***----------
Wavelength tunability is possible by many techniques like MMI coupler, external modulator due to thermal effects on the Mach - Zehnder modulator etc. Our this study demonstrates an easy method to achieve the wavelength tunability without much cumbersome technique discussed in the past. Our study reveals that by using S-bend curvature, we can achieve a smooth transition of power from one port to another port. We have used the standard parameters to design S-bend optical power splitter. This paper discusses the tunability without an external modulator. We have shown through the beam propagation method (BPM) simulation that 53 nm tunability extended from "O-band" to "E-band" as possible by our structure. Our study expected to be an accurate up to $\pm 2\ \%$ error. We have too carried out insertion loss, field propagation through the S-band structures. We have used the transparent boundary condition to avoid any back reflection at the boundary of the S-bend structure. Our waveguide structure maintains single mode operation at an entire structure. The experimental results show that, as the tilt angle increases the normalized optical power decreases for that arm. The results have been verified by MATLAB based simulation as well as OptiBPM software.

KEYWORDS: *Wavelength-tunable; symmetric waveguide; asymmetric waveguide; S-bend waveguide; beam propagation method.*

Date Of Submission: 16.July 2013, Date Of Publication: 25.July 2013

I. INTRODUCTION

Optical power dividers are essential and important components in optical integrated circuits. For various applications, input optical power is required to be distributed in several output waveguides with specified power-splitting ratio. According to the device structures, optical power dividers can be classified as three types: 1) branching waveguide; 2) directional coupler; and 3) multimode interference coupler. Among them, branching waveguides occupy the least device area and simultaneously have the flexibility of tunable power-splitting ratio and arbitrary power-splitting number. Curved waveguides are widely used in optical integrated circuits. Sasaki and Mikoshiba[1] shows that the conventional branch suffers severe radiation loss when the branching angle is larger than 2^{0}.

To reduce the radiation loss, the branching angle must be small and the device length is therefore increased. Several efforts have been made to overcome the loss problem, especially when the branching angle is large[2-3]. Brug et. al. measured and calculated S-bend excess loss, they also show that there is low loss in an S-bend waveguides as compared to straight waveguides.[4] Mustieles et. al. compared three typical S-bend profiles analytically and numerically and shows the bending losses at different iterations. They concluded that the bending losses evolution as a function of the number of iterations.[5] When a study has been conducted to see cross couplings in three types of S-bends, sine, cosine and double arc. It is seen that cosine S-bend offers the lowest cross coupling and variation in transition length in turn varies the slope of S-bends. It is seen that when the transition length is larger, more cross coupling of power occurs.[6] Tsuji et. al. described a finite element beam propagation method for both TE and TM waves propagating in strongly guiding and longitudinally varying optical directional coupler composed of two parallel identical waveguides, an S-bend, a Y-branching optical isolator, and a 4-ports optical circulator.[7] The beam propagation method (BPM) is at present the most widely used tools employed in the study of light propagation in longitudinally varying waveguides.[8-14] Hu[15] and Lu developed a practical procedure for calculating waveguide bends that preserve as much power as possible in the fundamental mode. The propagation of the wave field in the bend is calculated by a wide-angle BPM formulated in a curvilinear coordinate system.[16] The effective refractive index is reduced by increasing the rib height of the waveguide in the region between the output branches of Y-junction. The decrease in the effective refractive

index restricts the evanescent fields in this region and the incident power tends to remain in the output branches, therefore reducing the power loss.[17]

Low loss bending has been easily achieved by utilizing coherently coupled bends.[18-19] Jiang et. al. proposed and demonstrate a 1×2 thermooptic digital optical switch with variable optical attenuators that are integrated with the S-bend waveguides.[20] Solmaz et. al. have demonstrated a novel approach to improve the bending performance of titanium diffused $LiNbO_3$ waveguides using vertically integrated as S-bend waveguides.[21] Tao et. al. proposed an optical power splitter based on two parallel and identical spot-size mode converters. The mode converters are used to couple light directly from a lensed single-mode fiber, and lights in the mode converters are further separated with respective connecting S-bend waveguides.[22] Sahu has proposed a double S-bend lateral offset structure for the reduction of length and S-bend loss of 2×2 two mode interference (TMI) coupler.[23] Raghuwanshi et al. studied the Y-branch having inbuilt optical splitter and combiner using beam propagation method.[24] George et. al. proposed a compact integrated optical directional couplers with symmetrically and asymmetrically etched S-bend waveguides and shows that the directional couplers with asymmetrically etched waveguide structures can increase the device compactness to about 4 to 5 times that of the conventional symmetrically etched bend waveguide structures.[25] Zhao et. al. proposed an optical power splitter with one input and three output ports and demonstrated for near-infrared applications in the wavelength range of 2.3 to 2.5 μm.[26] Wei Li et. al. proposed a ultra-short 1×2 1310/1550 nm double-waveguide optical power splitter based on photonic crystal multimode interference. The device can be used to divide the input beam equally for both 1310nm and 1550nm at the same time.[27] Kumar et. al. proposed straight and S-bend rib waveguide structures with a novel design and characterized on a silicon-on-insulator (SOI) platform.[28] Tsao and Lu proposed the S-bend waveguide for attaching to the two kinds of SOI optical coupler and analyzed by BPM.[29] Wang et. al. proposed a wide-angle 1 x 3 optical power divider in $LiNbO_3$ for variable power splitting.[30] An important component for dense wavelength division multiplexing (DWDM) is low insertion loss, therefore Zhu et. al. described the designing and modeling of a wavelength-tunable ADM (Add/drop multiplexer) for DWDM.[31] Kim, and Song presented a tunable fiber-to-planar waveguide coupler based on the thermo-optic effect of a polymer film.[32]In this paper, we have presented the comparative study of the three different types S-bend waveguide optical beam splitter, regarding the optical power at two different waveguide arms, angle of splitting, the power loss at two different ports etc. Section 2 describes the theoretical aspects of the planar waveguide beam splitter. Section 3 explains about the beam propagation method. Section 4 explains about the construction of S-bend optical signal splitter. Section 5 describes the analysis between the actual data through software and approximate equation obtained from the vigorous analysis of the S-bend structure. Section 6 involves the study of behavior of power splitters for different wavelength input signal pulse. Finally concluded with results and discussion.

II. PLANAR WAVEGUIDE BEAM SPLITTER

A beam splitter is one of basic optical elements. It is widely used in both light and matter-wave optics. One important application of the beam splitters is inter-ferometry, which is important in many fundamental and applied measurements. In recent years the possibility of using beam splitters for producing entangled quantum states and in quantum teleportation has been actively discussed. Bends are often used to provide offset transitions at the input and output of devices, or separate guides at the edge of a chip for ease of coupling to fibers. In either case, an S-bend is used. The separation angle (A), distance between output ports (P), distance (D) between the straights and the bend radius (R) are related to the coupler's characteristics as shown in Fig. 1. The output pitch defines the length (L) of the coupler.

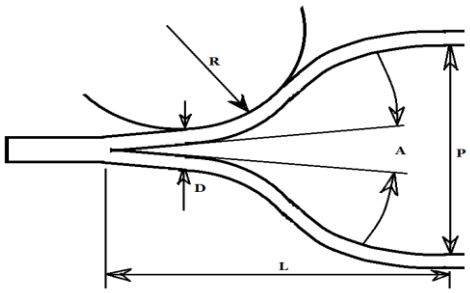

Fig. 1 Schematic view of S-bend waveguide beam splitter with physical parameters.

Power dividers are an important component to divide an optical signal into many branches in optical fiber subscriber networks. Figure 2(a), 2(b) and 2(c) shows the structural view of two branch waveguides corresponds to Fig. 1. The waveguide should have a small branching angle and a tapered part for maintaining the

fundamental mode propagation of the incident wave. The couplers are wavelength sensitive because their operation is based on phase matching. This property, we have used to an extend the tunability. Greater bandwidth and larger fabrication error tolerances can be obtained in couplers, which modified to have variable spacing.

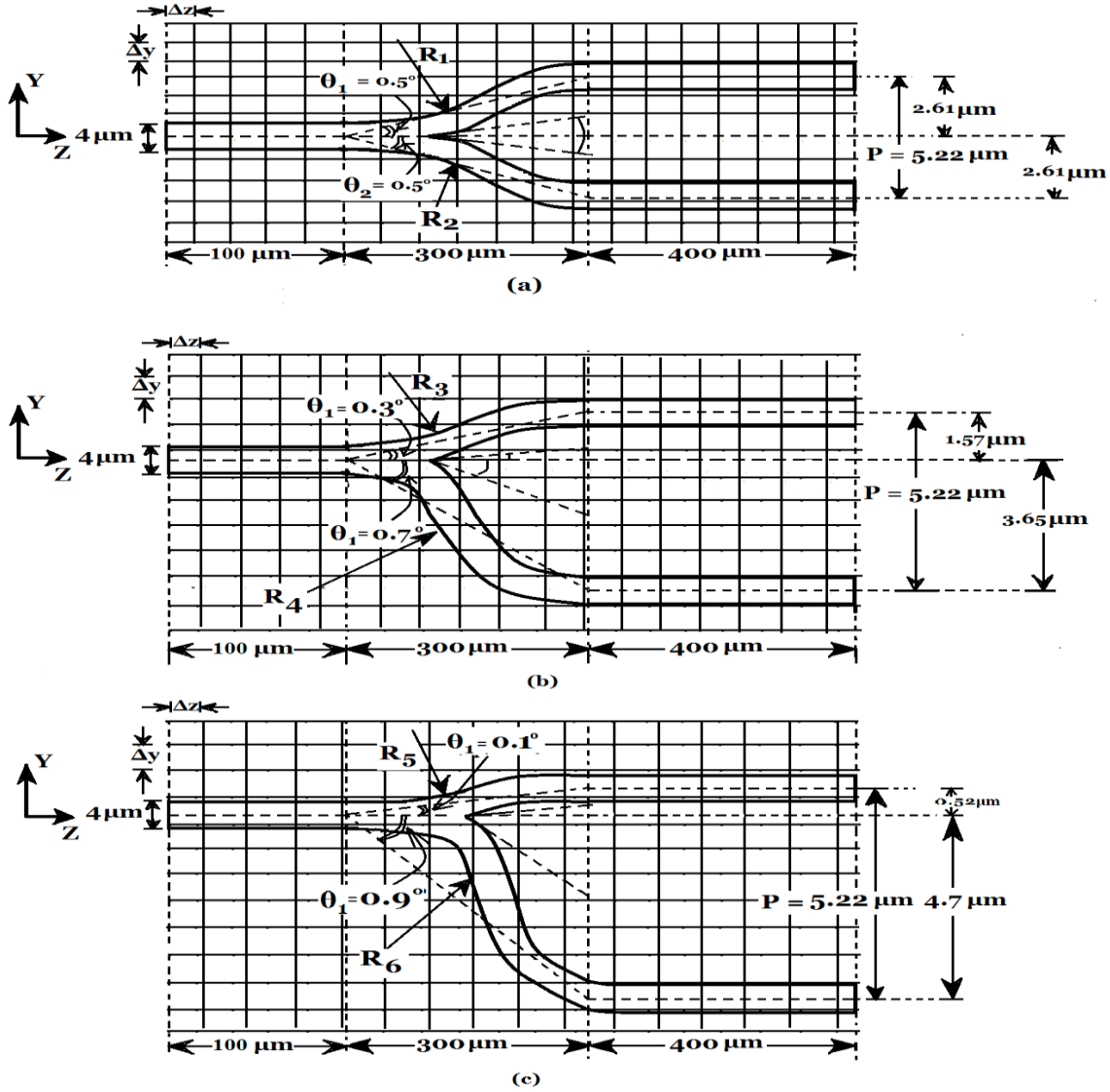

Fig. 2 Top view of basic structures of S-bend branching waveguides (a) symmetric (b) asymmetric, and (c) highly asymmetric two branches with proper dimension and tilt angles.

III. BEAM PROPAGATION METHOD (BPM): REVIEW

In this section, we have tried to formulate the problem as discussed in section 2 by using finite difference beam propagation method (FD-BPM). The FD-BPM is one of the most powerful techniques to investigate linear and nonlinear lightwave propagation phenomena such as branching and combining waveguides, S-shaped bend waveguides, and tapered waveguides. The first is that BPM is done entirely in the frequency domain, and as such only weak non-linearity can be modeled. The second is in the use of a slowly varying envelope approximation in the paraxial direction. In BPM, it is assumed that the device has an optical axis, and that most of the light travels in this direction, or at least approximately in this direction (paraxial approximation).[33-34] In BPM, as with the majority of literature on the subject, this axis is taken to be, the third space co-ordinate. Many practical optical devices are naturally aligned close to a single direction, so once this is associated with the axis, the slowly varying approximation can be applied. With regard to the branches, mode-

coupled and mode-transform types have been made to design a low-loss structure. For the Fig. 2, the wave equation for the x-directed electric field $E_y(x, y, z)$ after some manipulation is given by [35]

$$2j\beta \frac{\partial \emptyset}{\partial z} = \frac{\partial^2 \emptyset}{\partial y^2} + k_0^2(\varepsilon_r - n_{eff}^2)\emptyset \qquad (1)$$

Where in Eq. (1), k_0 is the wave number in the vacuum, $\emptyset(x, y, z)$ is field distribution modes, and n_{eff} is the reference index, for which the effective index is usually used. First, we discuss the FD expression for the Fresnel approximation. When we use the discretization of the y and z coordinates,

$$y = p\,\Delta y \qquad (2)$$

$$z = l\,\Delta z \qquad (3)$$

where p and l are integers, the following notations are used for the wave function $\emptyset(y, z)$ and the relative permittivity $\varepsilon_r(y, z)$ is given in [36]

$$\emptyset(y, z) \emptyset_p^{'} \qquad (4)$$

$$\varepsilon_r(y, z) \longrightarrow \varepsilon_r^{'}(p) \qquad (5)$$

The next step is the discretization of the Fresnel wave equation (1). First, we discretized it in the y-direction. The discretization number l, which corresponds to the z-coordinate, will be discussed later. The first and the second terms on the right-hand side of eq. (1) are expressed by using finite difference schemes as.

$$\frac{\partial^2 \emptyset}{\partial y^2} = \frac{\emptyset_{p+1} - 2\emptyset_p + \emptyset_{p-1}}{(\Delta y)^2} \qquad (6)$$

Where p is difference center

and

$$k_0^2(\varepsilon_r - n_{eff}^2)\emptyset = k_0^2[\varepsilon_r(p) - n_{eff}^2]\emptyset_p \qquad (7)$$

Substituting eqs. (6) and (7) into eq. (1), we get

$$2j\beta \frac{\partial \emptyset_p}{\partial z} = \frac{\emptyset_{p+1} - 2\emptyset_p + \emptyset_{p-1}}{(\Delta y)^2} + k_0^2[\varepsilon_r(p) - n_{eff}^2]\emptyset_p$$

$$= \alpha_w \emptyset_{p-1} + \alpha_y \emptyset_p + \alpha_e \emptyset_{p+1} + k_0^2[\varepsilon_r(p) - n_{eff}^2]\emptyset_p$$

Thus, the discretization of the wave equation (1) is

$$2j\beta \frac{\partial \emptyset_p}{\partial z} = \alpha_w \emptyset_{p-1} + \{\alpha_y + k_0^2[\varepsilon_r(p) - n_{eff}^2]\}\emptyset_p + \alpha_e \emptyset_{p+1} \qquad (8)$$

where, we used the definitions,

$$\alpha_w = \frac{1}{(\Delta y)^2} \qquad (9)$$

$$\alpha_e = \frac{1}{(\Delta y)^2} \qquad (10)$$

$$\alpha_y = -\frac{2}{(\Delta y)^2} \qquad (11)$$

The next step is the discretization of eq. (8) with respect to z. Discretizing the left hand side of eq. (8) with respect to z, we get,

$$2j\beta \frac{\emptyset_p^{l+1} - \emptyset_p^l}{\Delta z} \qquad (12)$$

It should be noted that, as shown in expression (12), the difference center of the left-hand side of eq. (8) is the point $l + \frac{1}{2}$ midway between l and $l + 1$. The difference center of the right-hand side of eq. (8) discretized with respect to z should be $l + \frac{1}{2}$. Thus, we modify eq. (8) to

$$2j\beta \frac{\emptyset_p^{l+1} - \emptyset_p^l}{\Delta z} = \frac{1}{2}[\alpha_w^l \emptyset_{p-1}^l + \{\alpha_y^l + k_0^2[\varepsilon_r^{'}(p) - n_{eff}^2]\}\emptyset_p^l + \alpha_e^l \emptyset_{p+1}^l]$$

$$+ \frac{1}{2}[\alpha_w^{l+1} \emptyset_{p-1}^{l+1} + \{\alpha_y^{l+1} + k_0^2[\varepsilon_r^{l+1}(p) - n_{eff}^2]\}\emptyset_p^{l+1} + \alpha_e^{l+1} \emptyset_{p+1}^{l+1}] \qquad (13)$$

Rewriting this equation so that the terms on the left and right hand sides respectively contain $l + 1$ and l, we get,

$$-\frac{\alpha_w^{l+1}}{2} \emptyset_{p-1}^{l+1} + \left\{\frac{-\alpha_y^{l+1}}{2} + \frac{2j\beta}{\Delta z} - \frac{1}{2} k_0^2[\varepsilon_r^l(p) - n_{eff}^2]\right\} \emptyset_p^{l+1} - \frac{\alpha_e^{l+1}}{2} \emptyset_{p+1}^{l+1}$$

$$= \frac{\alpha_w^l}{2}\varnothing_{p-1}^l + \left\{\frac{\alpha_y^l}{2} + \frac{2j\beta}{\Delta z} + \frac{1}{2}k_0^2\left[\varepsilon_r^l(p) - n_{eff}^2\right]\right\}\varnothing_p^l + \frac{\alpha_e^l}{2}\varnothing_{p+1}^l$$

multiplying both sides of this equation by 2, we get the FD expression for TE mode:

$$-\alpha_w^{l+1}\varnothing_{p-1}^{l+1} + \left\{-\alpha_y^{l+1} + \frac{4j\beta}{\Delta z} - k_0^2\left[\varepsilon_r^{l+1}(p) - n_{eff}^2\right]\right\}\varnothing_p^{l+1} - \alpha_e^{l+1}\varnothing_{p+1}^{l+1}$$

$$= \alpha_w^l\varnothing_{p-1}^l + \left\{\alpha_y^l + \frac{4j\beta}{\Delta z} + k_0^2\left[\varepsilon_r^l(p) - n_{eff}^2\right]\right\}\varnothing_p^l + \alpha_e^l\varnothing_{p+1}^l \qquad (14)$$

Although in eq. (14) we use the wave number in a vacuum, k_0, for ease of understanding, it is recommended that in actual programming the coordinates (i.e., x, y, and z) be multiplied by k_0 and the propagation constant β be divided by k_0 in order to reduce the round-off errors. The resulting formulation corresponds to dividing both sides of eq. (14) by k_0^2. We have computed the effective index or modal index by using the effective index method.[37] It is verified by software as shown in Fig. C (Appendix), therefore at $\lambda = 1330$ nm, $n_{eff} = 1.48674$.In this algorithm, we have discretized the whole 2-D region of the structure. The length and the width of the wafer structure is 800 μm and 20 μm respectively. The length of the wafer section (along the z-axis) is divided into 1000 no. of discretized section and width is divided into 500 discretized sections. By reducing Δy and Δz, we can improve the accuracy of algorithm. Our BPM simulation converges well for chosen value of Δy andΔz. Thus, we can write,

$$\left.\begin{array}{l}\Delta y = 0.04\ \mu m \quad p = 0 \rightarrow 500\\ \Delta z = 0.8\ \mu m \quad l = 0 \rightarrow 1000\end{array}\right\}; \text{p, l are integers} \qquad (15)$$

Now, we have derived the equation by FD BPM as follow;

$$-\alpha_w^{l+1}\varnothing_{p-1}^{l+1} + \left\{-\alpha_y^{l+1} + \frac{4j\beta}{\Delta z} - k_0^2\left[\varepsilon_r^{l+1}(p) - n_{eff}^2\right]\right\}\varnothing_p^{l+1} - \alpha_e^{l+1}\varnothing_{p+1}^{l+1}$$

$$= \alpha_w^l\varnothing_{p-1}^l + \left\{\alpha_y^l + \frac{4j\beta}{\Delta z} + k_0^2\left[\varepsilon_r^l(p) - n_{eff}^2\right]\right\}\varnothing_p^l + \alpha_e^l\varnothing_{p+1}^l \qquad (16)$$

In the above equation (16) we have assumed that,

$$\alpha_w = \frac{1}{(\Delta y)^2}, \quad \alpha_y = -\frac{2}{(\Delta y)^2}, \quad \alpha_e = \frac{1}{(\Delta y)^2}, \quad \beta = \frac{2\pi}{\lambda}n_{eff} \qquad (17)$$

For the efficient matrix representation of eq. (16) we can assume

$$A_p = \alpha_y^l + \frac{4j\beta}{\Delta z} + k_0^2\left[\varepsilon_r^l(p) - n_{eff}^2\right],\ B_p = -\alpha_y^{l+1} + \frac{4j\beta}{\Delta z} - k_0^2\left[\varepsilon_r^{l+1}(p) - n_{eff}^2\right].$$

The equation (16) can be represented in the form of the matrix as follow.

$$\begin{bmatrix} -\alpha_w^{l+1} & \cdots & 0 \\ 0 & \ddots & \\ \vdots & B_p & \vdots \\ & \ddots & \\ 0 & \cdots & -\alpha_e^{l+1} \end{bmatrix} \begin{bmatrix} \phi_0^{l+1} \\ \phi_1^{l+1} \\ \vdots \\ \phi_{250}^{l+1} \\ \vdots \\ \phi_{500}^{l+1} \end{bmatrix}$$

$$= \begin{bmatrix} \alpha_w^l & \cdots & 0 \\ 0 & \ddots & \\ \vdots & A_p & \vdots \\ & \ddots & \\ 0 & \cdots & \alpha_e^l \end{bmatrix} \begin{bmatrix} \phi_0^l \\ \phi_1^l \\ \vdots \\ \phi_{250}^l \\ \vdots \\ \phi_{500}^l \end{bmatrix} \qquad (18)$$

Now, from equation (18) we can write;

$$\begin{bmatrix} \phi_0^{l+1} \\ \phi_1^{l+1} \\ \vdots \\ \phi_{250}^{l+1} \\ \vdots \\ \phi_{500}^{l+1} \end{bmatrix} = \begin{bmatrix} \alpha_w^l & \cdots & 0 \\ 0 & \ddots & \\ \vdots & A_p & \vdots \\ & \ddots & \\ 0 & \cdots & \alpha_e^l \end{bmatrix} \begin{bmatrix} -\alpha_w^{l+1} & \cdots & 0 \\ 0 & \ddots & \\ \vdots & B_p & \vdots \\ & \ddots & \\ 0 & \cdots & -\alpha_e^{l+1} \end{bmatrix}^{-1} \begin{bmatrix} \phi_0^l \\ \phi_1^l \\ \vdots \\ \phi_{250}^l \\ \vdots \\ \phi_{500}^l \end{bmatrix} \quad (19)$$

But in order to write the algorithm, it is necessary to write the expression for the $\varepsilon_r(p) = n^2(p)$. Where n is the refractive index of the structures with respect to length and width. The variation can be represented as follows:

Ranges of ε_r for Symmetric, Asymmetric and Highly Asymmetric S-Bend structure

For $z = 0\ \mu m$ to $100\ \mu m$ or $0 \le l \le 125$ (This region is identical for all the S-bend structures)

$$\varepsilon_r = \begin{cases} (1.5)^2 & -2\ \mu m \le y \le 2\mu m \text{ or } 200 \le p \le 300 \\ (1.48)^2 & \text{otherwise} \end{cases} \quad (20)$$

For $z = 100.8\ \mu m$ to $400\ \mu m$ or $126 \le l \le 500$, $(i,j) = \begin{cases} (1,2) \rightarrow \text{Symmetric Sructure} \\ (3,4) \rightarrow \text{Asymmetric Structure} \\ (5,6) \rightarrow \text{Highly Asymmetric Structure} \end{cases}$

$$\varepsilon_r = \begin{cases} (1.5)^2 & R_j(z) \le y \le R_j(z) + 4\mu m \text{ or } \dfrac{10 - |R_j(z)|}{0.04} \le p \le \dfrac{10 - |R_j(z) + 4\ \mu m|}{0.04} \\ (1.5)^2 & R_i(z) - 4\mu m \le y \le R_i(z) \text{ or } \dfrac{10 + |R_i(z) - 4|}{0.04} \le p \le \dfrac{10 + |R_i(z)|}{0.04} \\ (1.48)^2 & \text{otherwise} \end{cases} \quad (21)$$

For $z = 400.8\ \mu m$ to 800 or $501 \le l \le 1000\ \mu m$ (For Symmetric S − bend structure)

$$\varepsilon_r = \begin{cases} (1.5)^2 & -4.61\ \mu m \le y \le -0.61\ \mu m \text{ or } 135 \le p \le 235 \\ (1.5)^2 & 0.61\ \mu m \le y \le 4.61\mu \text{ or } 265 \le p \le 365 \\ (1.48)^2 & \text{otherwise} \end{cases} \quad (22)$$

For $z = 400.8\ \mu m$ to 800 or $501 \le l \le 1000\ \mu m$ (For an Asymmetric S − bend structure)

$$\varepsilon_r = \begin{cases} (1.5)^2 & -5.65\ \mu m \le y \le -1.64\ \mu m \text{ or } 109 \le p \le 209 \\ (1.5)^2 & -0.43\ \mu m \le y \le 3.57\ \mu m \text{ or } 239 \le p \le 339 \\ (1.48)^2 & \text{otherwise} \end{cases} \quad (23)$$

For $z = 400.8\ \mu m$ to 800 or $501 \le l \le 1000\ \mu m$ (For Highly Asymmetric Structure)

$$\varepsilon_r = \begin{cases} (1.5)^2 & -6.7\ \mu m \le y \le -2.7\ \mu m \text{ or } 83 \le p \le 183 \\ (1.5)^2 & -1.48\ \mu m \le y \le 2.52\ \mu m \text{ or } 213 \le p \le 313 \\ (1.48)^2 & \text{otherwise} \end{cases} \quad (24)$$

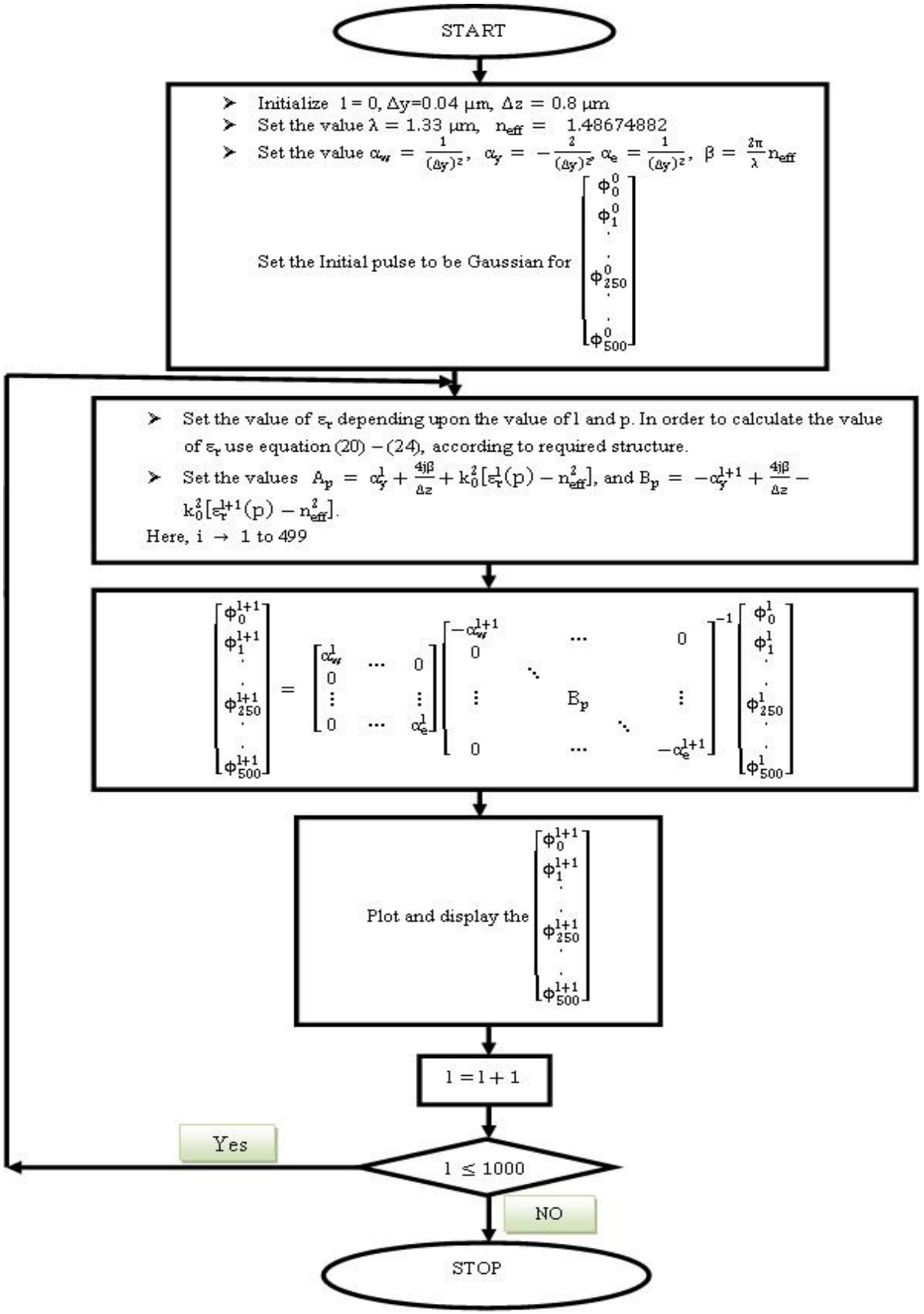
START
Initialize l = 0, Δy=0.04 μm, Δz = 0.8 μm
Set the value λ = 1.33 μm, n_{eff} = 1.48674882
Set the value $\alpha_{ss} = \frac{1}{(\Delta y)^2}$, $\alpha_y = -\frac{2}{(\Delta y)^2}$, $\alpha_e = \frac{1}{(\Delta y)^2}$, $\beta = \frac{2\pi}{\lambda} n_{eff}$
Set the Initial pulse to be Gaussian for $\begin{bmatrix} \phi_0^0 \\ \phi_1^0 \\ \vdots \\ \phi_{250}^0 \\ \vdots \\ \phi_{500}^0 \end{bmatrix}$
Set the value of ε_r depending upon the value of l and p. In order to calculate the value of ε_r use equation (20) – (24), according to required structure.
Set the values $A_p = \alpha_y^l + \frac{4j\beta}{\Delta z} + k_0^2[\varepsilon_r^l(p) - n_{eff}^2]$, and $B_p = -\alpha_y^{l+1} + \frac{4j\beta}{\Delta z} - k_0^2[\varepsilon_r^{l+1}(p) - n_{eff}^2]$.
Here, i → 1 to 499
$\begin{bmatrix} \phi_0^{l+1} \\ \phi_1^{l+1} \\ \vdots \\ \phi_{250}^{l+1} \\ \vdots \\ \phi_{500}^{l+1} \end{bmatrix} = \begin{bmatrix} \alpha_{ss}^l & \cdots & 0 \\ 0 & & \\ \vdots & & \vdots \\ 0 & \cdots & \alpha_e^l \end{bmatrix} \begin{bmatrix} -\alpha_{ss}^{l+1} & \cdots & 0 \\ 0 & \ddots & \\ \vdots & B_p & \vdots \\ & \ddots & \\ 0 & \cdots & -\alpha_e^{l+1} \end{bmatrix}^{-1} \begin{bmatrix} \phi_0^l \\ \phi_1^l \\ \vdots \\ \phi_{250}^l \\ \vdots \\ \phi_{500}^l \end{bmatrix}$
Plot and display the $\begin{bmatrix} \phi_0^{l+1} \\ \phi_1^{l+1} \\ \vdots \\ \phi_{250}^{l+1} \\ \vdots \\ \phi_{500}^{l+1} \end{bmatrix}$
l = l + 1
Yes
l ≤ 1000
NO
STOP

IV. SIMULATION RESULTS OF S-BEND OPTICAL POWER SPLITTER

In optical communication system, power dividers are amongst those devices for which there is no substitute. The waveguide power divider can be in the form of branches and directional couplers. In contrast to branches, dividers using directional couplers easily to achieve low-loss characteristics, although wavelength dependency might be expected. Figure 3 shows the simulation results for the layout of Fig. 2 (a) of the symmetric S-bend optical power splitter. In this layout, length of the device is 800 μm and the width of all the sections of this waveguide device is selected as $4\mu m$. This figure also shows the normalized output power implemented in MATLAB with respect to the length and the width of the waveguide, which provides the essential ideas for analyzing these power dividers. The waveguide is investigated; whose core and cladding refractive indices are 1.50 and 1.48 respectively. We treat the case with$(n_{CO}/n_{CL} = 1.0135)$. Where n_{CO} and n_{CL} are refractive indices of the core and cladding. Here, there is less difference between the refractive index of the core and cladding, therefore it acts as single mode waveguide structures. In general, it is difficult to realize equal power division by simply arranging the two output waveguides. Therefore, by arranging the tilt angle with equal amount, and the total angle of separation between the two arms, should be less than 1^0, we can get the proper result of equal power division. In the case of symmetric S-bend optical power splitter the tilt angle of the two arms of the waveguide devices is 0.5^0 each because, the coupled type divider composed of tilted waveguides.

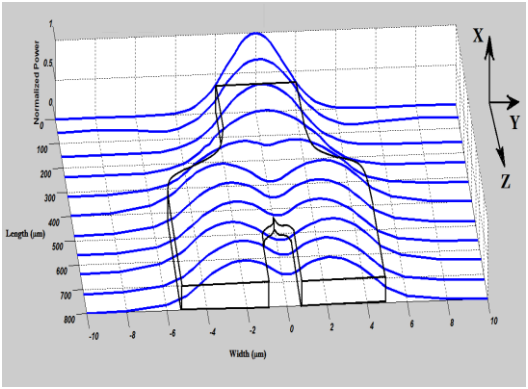

Fig. 3 Normalized power at various lengths of symmetric S-bend optical power splitter for the case of Fig. 2(a) at $\lambda = 1.33\ \mu m$.

The power ratio amongst the waveguide depends on the coupling strength. Here, we are using excess loss $= -10\log[(P_1 + P_2)/P_0]$ and insertion loss at port-I $= -10\log(P_1/P_0)$, insertion loss at port-II $= -10\log(P_2/P_0)$, where P_0 is input power, P_1 is power at port I, and P_2 is power at port II.

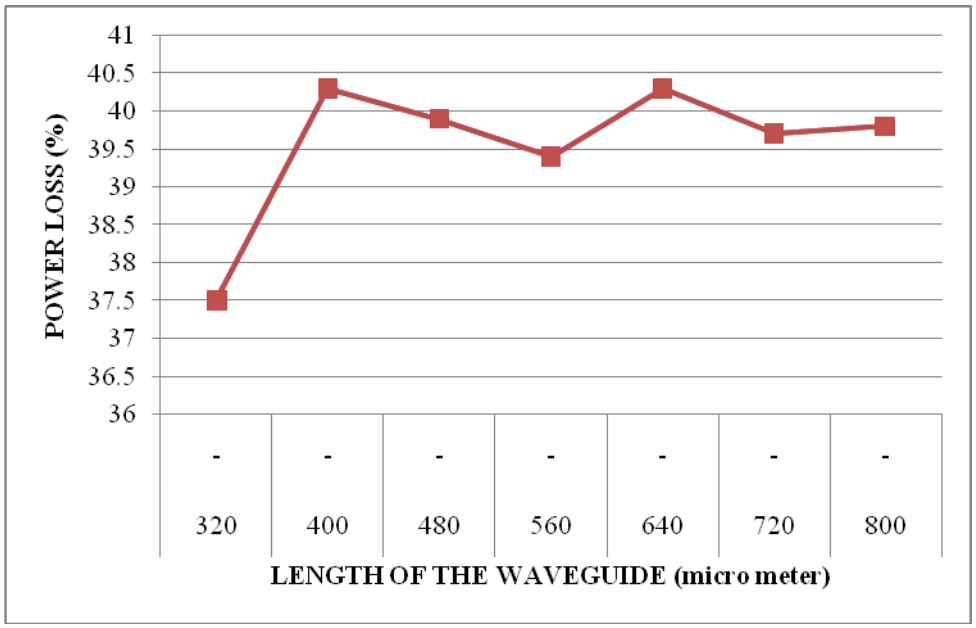

(a)

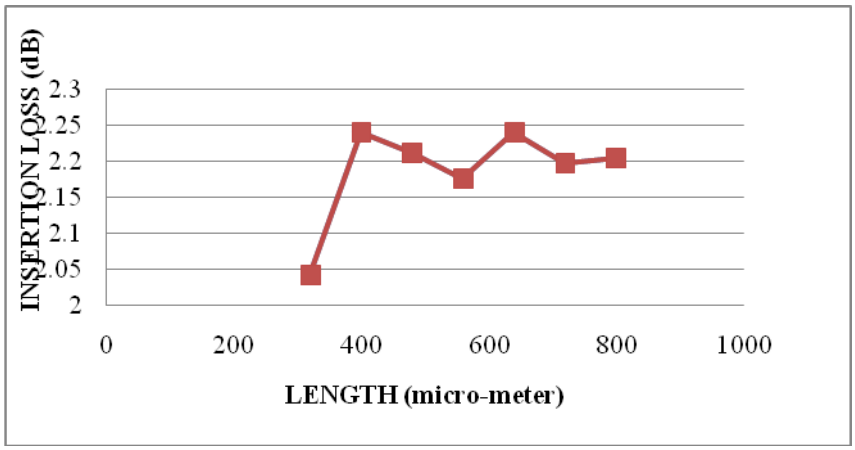

(b)

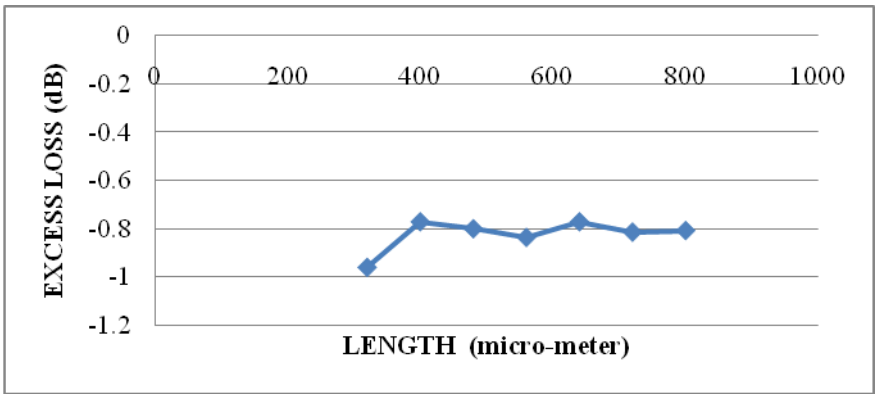

(c)

Fig. 4 (a) Power losses (b) insertion losses, (c) excess loss for both ports in symmetric S-bend structure at $\lambda = 1.33\ \mu m$.

Basically, the Fig. 4 shows the variation of the power loss, insertion loss and excess loss along the length and the width of the devices. We can analyze that the normalized power value decreases along the length of the devices. The power split with equal amount in the both arms along the length of the devices. Now as the tilt angle θ_1 and θ_2 varies the waveguide spacing with respect to origin varies, the amount of normalized optical power also varies. Optical power dividers are essential and important components in optical integrated circuits. For various applications, input optical power is required to be distributed in several output waveguides with specified power-splitting ratio. Figure 5 shows the normalized power at various lengths of asymmetric S-bend optical power as shown in Fig. 2(b). This figure includes MATLAB plot representing the normalized power in the form of the Gaussian pulses.

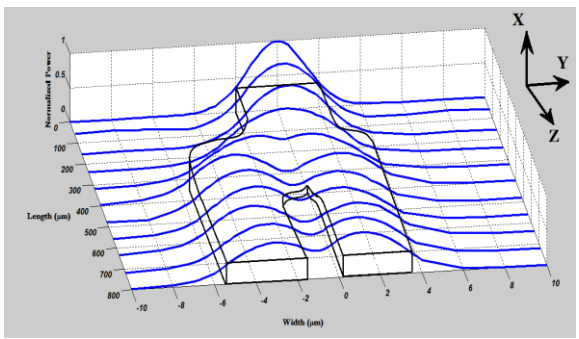

Fig. 5 Normalized power at various lengths of asymmetric S-bend optical power splitter for the case of Fig. 2(b) at $\lambda = 1.33\ \mu m$.

Now, the normalized power is analyzed at various important points of the waveguide along its length. Figure 6 shows the quantitative analysis of the asymmetric waveguide, containing all the important parameters such that the value of the normalized power inside the linear waveguide, the S-bend optical power arms, the losses of the signal at various stages, insertion loss at the two output ports and excess loss. The quantitative analysis represents that at the end of the waveguide the power is divided by unequally. More precisely, we can say that the output arm which is less tilted (output arm I, $\theta_1 = 0.3^0, \theta_2 = 0.7^0$) contains the most amount of normalized power in comparison to the other larger tilt of angle waveguide. Fig. 6 (a) and 6 (b) shows that coupling of both the arms are occurred at $697\ \mu m$.

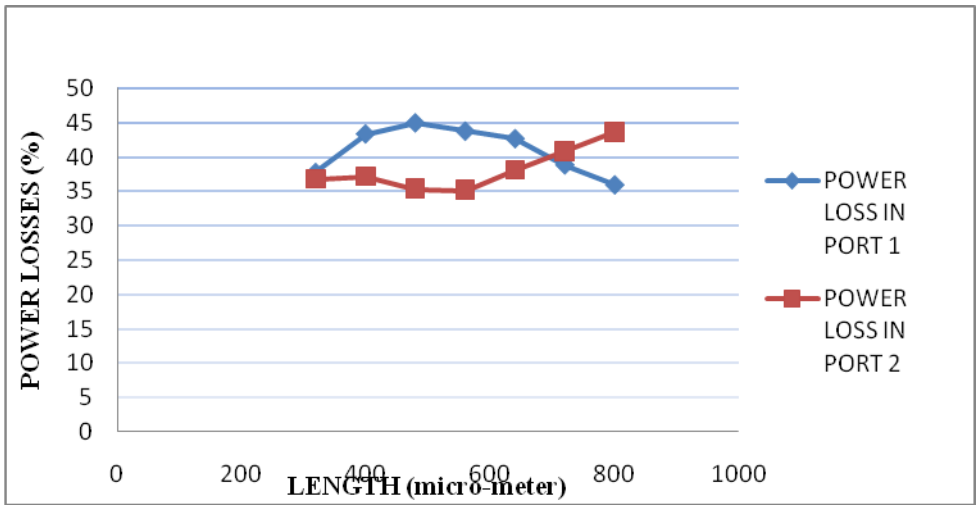

(a)

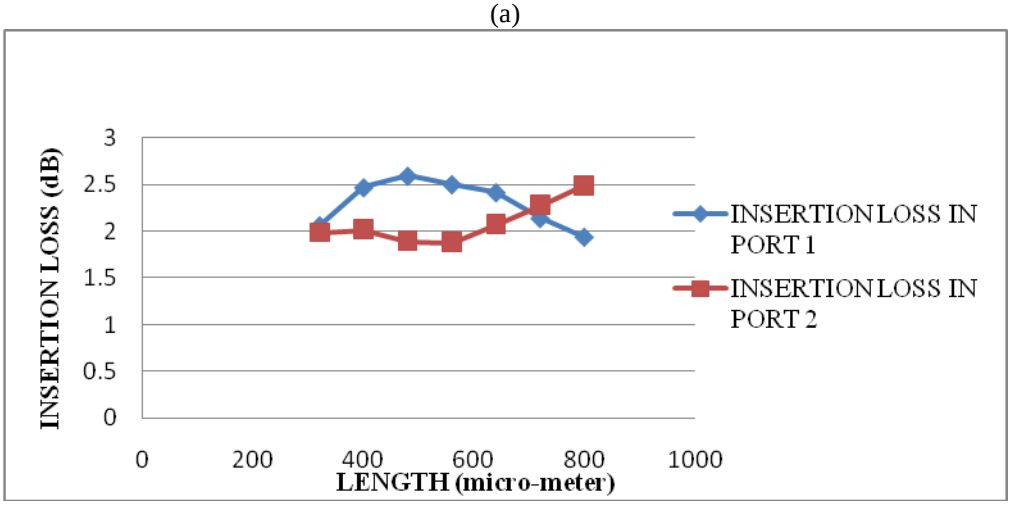

(b)

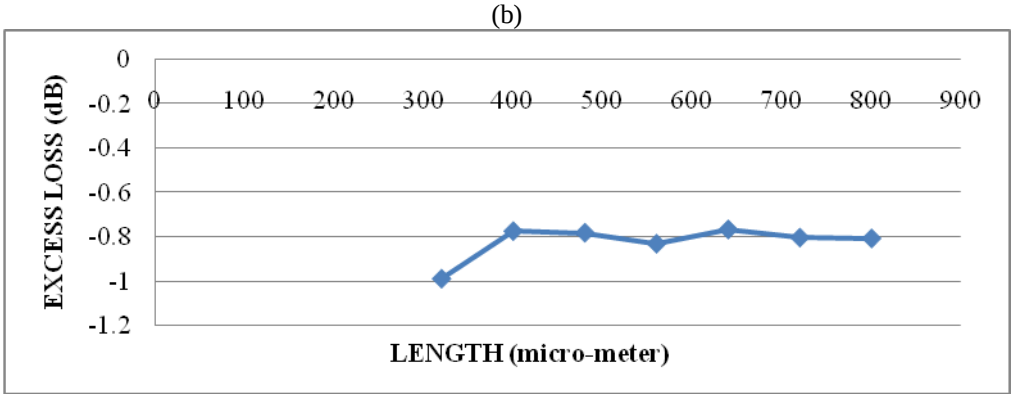

(c)

Fig. 6 (a) Power losses (b) Insertion losses, (c) excess loss for both ports in asymmetric S-bend structure at $\lambda = 1.33\ \mu m$.

Based on the same concept, the same analysis for the highly asymmetric optical power splitter has done. In this case, some more tilt has been introduced in output arm-II in comparison to the output arm- I. The main objective is to analyze the normalized output power in each arm. Figure 7 represents the basic view of a highly asymmetric waveguide. It also includes the normalized output power in the form of the Gaussian pulses, which shows the clear and expressive view of power at each stage of the optical power splitter in the case of the highly asymmetric waveguide. In this case, we have introduced the tilt angle of $\theta_1 = 0.1^0$ and $\theta_2 = 0.9^0$.

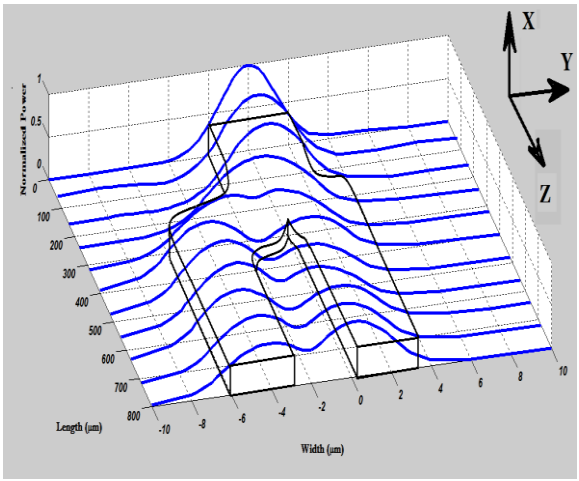

Fig. 7 Normalized power at various lengths of highly asymmetric S-bend optical power splitter for the case of Fig. 3(c) at $\lambda = 1.33\ \mu m$.

The quantitative analysis shows that, the decrement of normalized power as it traverses through the waveguides. After a certain length the power starts to split up to the length of $800\ \mu m$. This analysis shows that, as the tile angle is reduced for port – I and increased for the port – II, some more amount of normalized power is contributed to the output port – I in comparison to the previous asymmetric optical power splitter. Fig. 8 (a) and 8 (b) shows that coupling of both the arms are occurred at $724\ \mu m$, therefore from Fig. 6 and 8, we can observe that distance of coupling are increases, when asymmetricity are increases.

For the vigorous analysis, we have obtained the value of the normalized output power at both the port for all possible value of the tilt angle θ_1. In order to justify the theory, Fig. 9 shows the variation of the power in port – I and port – II at $\lambda = 1.33\ \mu m$. Figures 5 to 9 has to be computed at other wavelengths also for the purpose to show tunability.

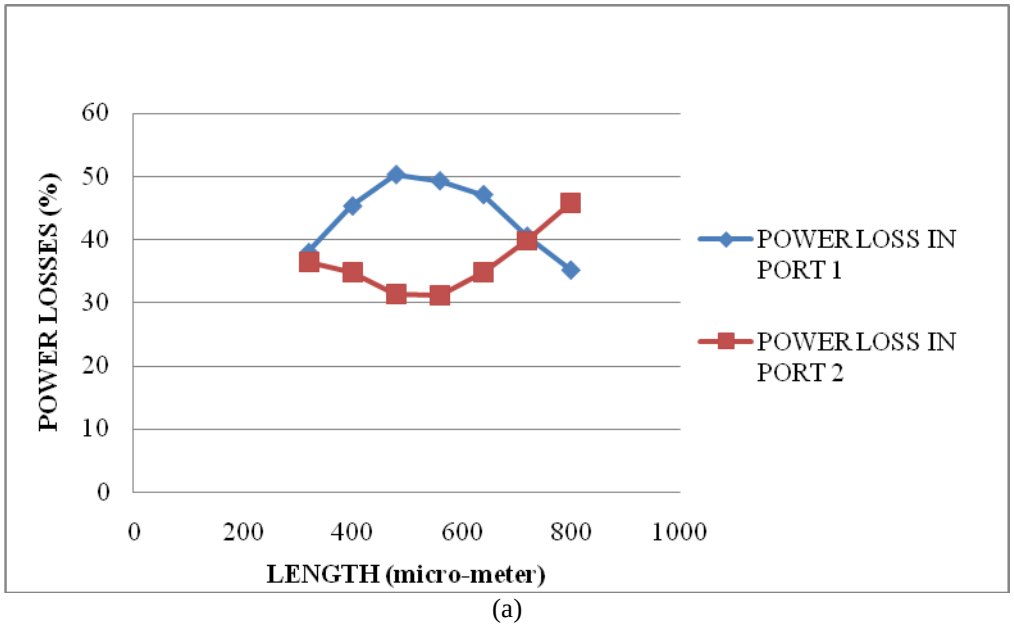

(a)

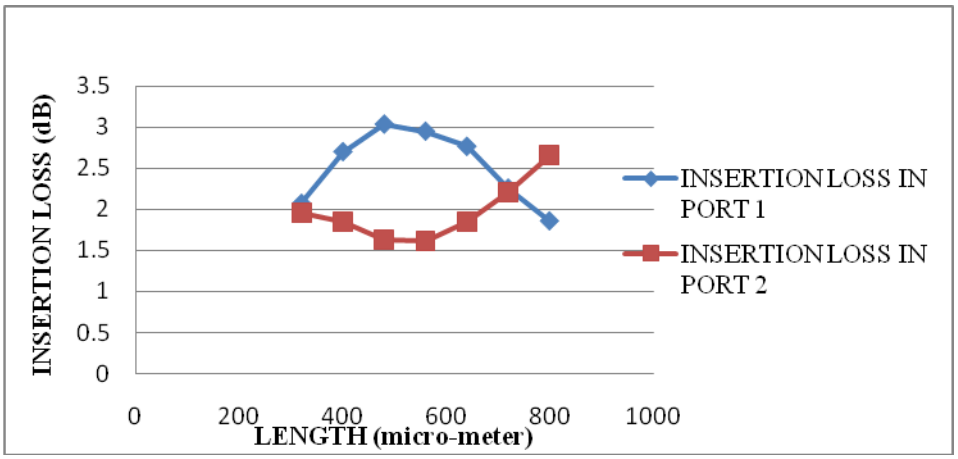

(b)

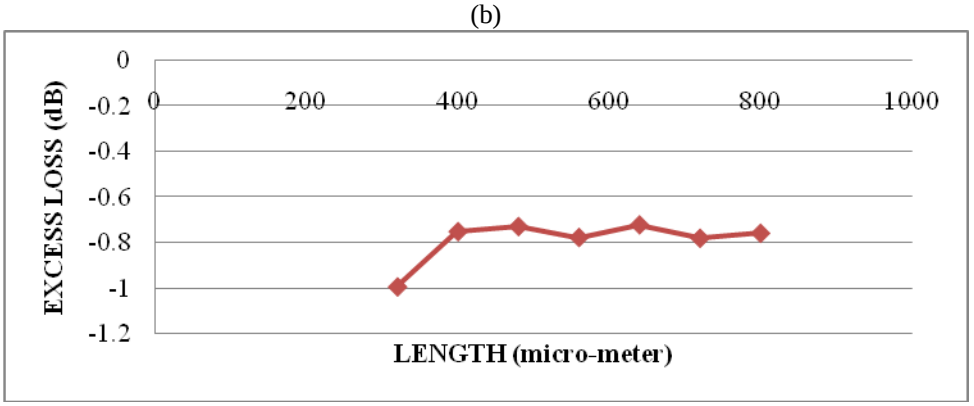

(c)

Fig. 8 (a) Power losses (b) insertion losses, (c) excess loss for both ports in highly asymmetric S-bend structure at $\lambda = 1.33\ \mu m$.

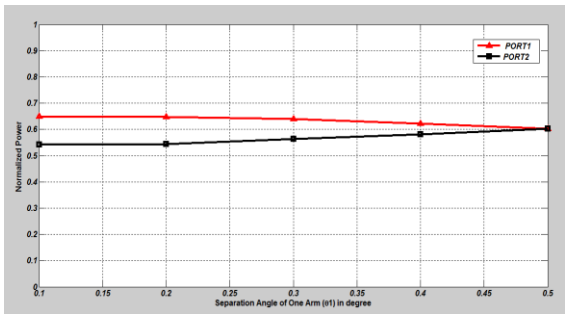

Fig. 9 Variation of power at two different arms with respect to the angle θ_1 (angle of separation of Port 1)

V. RESULTS VERIFICATION BY OPTI-BPM SOFTWARE

In this section, we discuss about the construction of S-bend optical signal splitter using Opti-BPM 11 software developed by Opti-Wave Corporation. The construction of the device consists of various steps. First of all defining the appropriate material is one of the important aspects. Basically, this section describes the physical and compositional properties of the wafer, waveguides, various dielectric materials, channels etc. Wafer is set at the beginning of the creation of a project because they are expected to change less frequently. For example, it is expected that a property such as the refractive index will change less frequently in a design session than any other property that is to be engineered, such as layout geometry. The waveguide profile is the specification of the waveguide geometry in the transverse plane. Channel waveguides consist of layers, fibers have a circular cross section, and diffused waveguides have graded index. These definitions also change less often in a design

session than layout geometry. The dielectric material is silica core and silica cladding, which refractive index is 1.5 and 1.48 respectively.

The layout setting is defined by the appropriate parameter and dimension selection of default waveguide. We have selected the width of the waveguide as $4\ \mu m$. Both the default setting and the association of any individual waveguide can be changed at any time. For, the creation of the S-bend optical beam splitter we have selected the length and width of the wafer dimension as $800\ \mu m$ and $20\ \mu m$ respectively. Now, the waveguide is created and observed for three types of structure mainly, (i) symmetric (ii) asymmetric and (iii) highly asymmetric S-bend optical splitter.

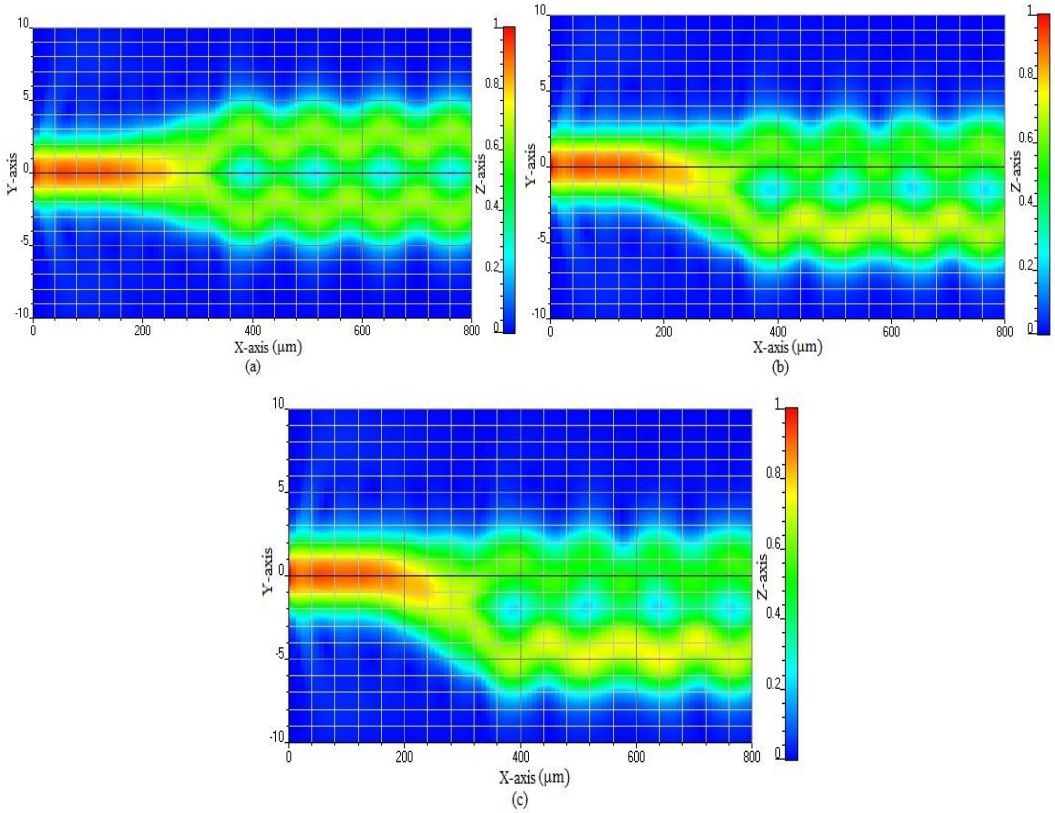

Fig. 10 Optical field propagation through (a) symmetric (b) asymmetric, and (c) highly asymmetric S-bend optical power splitter.

Fig. 10 shows optical field propagation through (a) symmetric (b) asymmetric, and (c) highly asymmetric S-bend optical power splitter. In Fig. 10 (a), angle between arm is 1^0 and both arms are symmetric means angle between the arm and X-axis is 0.5^0. So, power divides equally in the both arms. Fig. 10 (b) shows the asymmetric optical power splitter, because the angle between the arm and X-axis are 0.3^0 and 0.7^0. Here, we can observe that more power is transmitted in the arm of lesser angle. Similarly, Fig. 10 (c) shows the highly asymmetric optical power splitter because the angle between arms and X-axis are 0.1^0 and 0.9^0. Again, we can observed that more power is transmitted with the arm of lesser angle.

VI. DEMONSTRATION OF WAVELENGTH TUNABILITY DUE TO OUR PROPOSED STRUCTURE

This section involves the study of behavior of power splitters for different wavelength input signal pulse. It is interesting to study the wavelength tunability due to S-bend power splitter. Due to the variation in the wavelength of the input signal, S-bend power splitter shows different responses. Figure 11 shows the graphical view of input-output signal variation for different wavelength input signal along the width of the power splitter. It is an apparent that, in case of symmetric S-bend power splitter, the normalized power attains the same value but decreases as the wavelength of the input signal increases from O-band (1260nm – 1360 nm) to L-band (1565 nm – 1625 nm). However, it is also apparent from this figure that for the case of asymmetric structures, the

maximum power alters from port-II at lower wavelengths to port-I at higher wavelengths. Indeed, this functionality can be used to achieve the tunability and 3-dB power divider system.

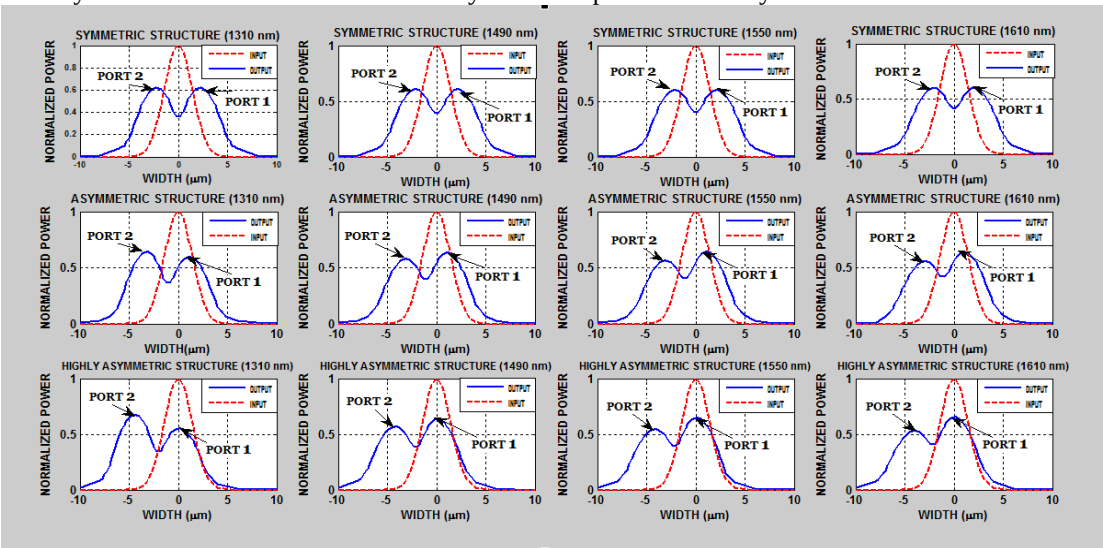

Fig. 11 Response at $Z = 800\ \mu m$ of various S-bend power splitter over the different wavelength (1310 nm, 1490 nm, 1550 nm and 1610 nm) input signal pulse at $Z = 0\ \mu m$.

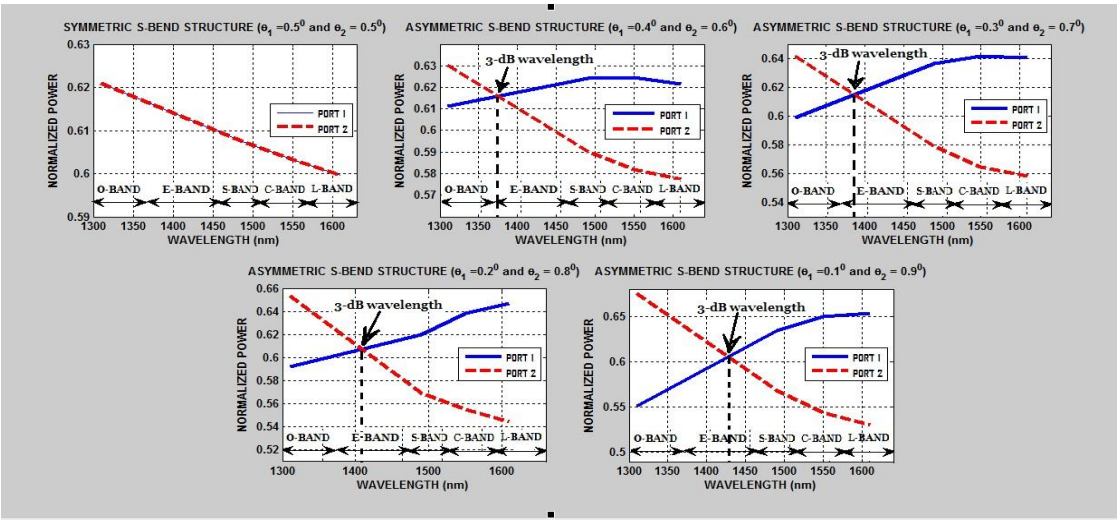

Fig. 12 Variations of normalized output power at the ports of symmetric and asymmetric structures.

Appendix B represents the required optical band that needs to be considered in the proper analysis of the all types S-band structures. Figure 12 reflects the variation of the normalized power on the two ports of the various S-bend power splitters across the various bands of signals. Figure 12 represents that normalized output power increase in port I and decreases at the port II with increment in the wavelength of the input signal from O-band to E-band, in case asymmetric and highly asymmetric S-bend optical power splitter. It also represents that in an O - band (1310 nm), the normalized power acquires the higher value in port II with respect to port I for an asymmetric to highly asymmetric S-bend optical power splitter. Subsequently, the normalized power decreases with port II and increases on port I as the wavelength of the input signal pulse increases form O-band to L-band. We can conclude that, as the S-bend structure becomes more and more asymmetric, the difference in the normalized power at port I and port II increases. Therefore, it shows that in C- and L- band more amount of normalized power occurs at the port I with respect to port II. Hence, it reflects an asymmetric structure also involves the equal power distribution at a particular wavelength. The analysis suggests that, the particular wavelength (3 dB wavelengths or equal power division wavelength) at which the asymmetric structure shows the equal power distribution shifts from O-band to L-band, as the S-bend structure becomes more and more asymmetric. Asymmetric structure shows the equal power distribution at 1372 nm, when the angle of tilt is

$(\theta_1 = 0.4^0, \theta_2 = 0.6^0)$, at 1363 nm, when the angle of tilt is $(\theta_1 = 0.3^0, \theta_2 = 0.7^0)$, at 1402 nm, when the angle of tilt is $(\theta_1 = 0.2^0, \theta_2 = 0.8^0)$ and at 1425 nm, when the angle of tilt is $(\theta_1 = 0.1^0, \theta_2 = 0.9^0)$.

Therefore, we are proposing the structures of 53 nm wavelength tunability. The above discussion shows that by adjusting the wavelength of the input signal we can vary the proportion of power at two ports of the S-bend structures. Figure 13 shows the plot of the 3-dB wavelength or equal power division wavelength variation with the angle of tilt of port I and port II. It also shows the effect of the asymmetricity over mid band wavelength. This property can be used to design a wave tunable source of around 68 nm bandwidth as shown in Fig. 13. This tunability bandwidth is quite substantial for all practical applications of fiber. As we know by ITU-T, recommended channel spacing for dense wavelength division multiplexing (DWDM) system is 100 GHz ≈ 0.8 nm; hence for this bandwidth around 90 channels can be accommodated for tunability.

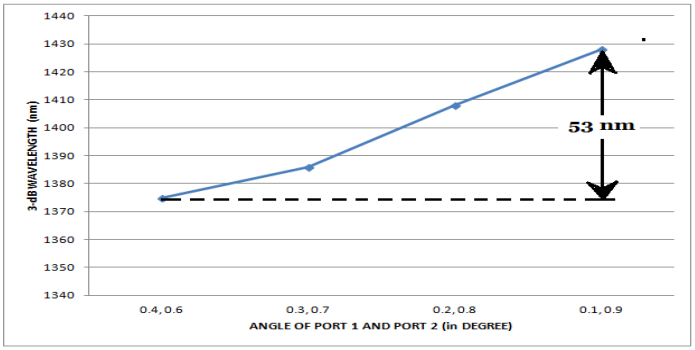

Fig. 13 Variations of the mid-band wavelength with respect to the tilt angle of port 1.

The modal index or effective index of the waveguide is the parameter that can be changed due to the structural variation and the wavelengths of the applied input signal. In Appendix Fig. C shows the modal index variation with respect to the wavelengths of the applied input signal for all the three structures. This property, we have used to design our own algorithm. As in our formulations "n_{eff}" is unknown, which has been found by an effective index method for 3-D waveguide structure. The results have been verified by OptiBPM software. This diagram also shows that the effective modal index decreases with respect to the wavelengths for all the three types of structure. Hence, as the wavelength of the input signal structures increases the modal index of all the S-bend structures decreases. n_{eff} is changed for significantly for our study at 1320 nm and 1600 nm wavelength.

VII. CONCLUSION

In this paper, we have investigated the importance of S-Bend optical beam splitter in the modern technological perspective. We found that the tilt angle of the output arms for these types of devices plays an important role in dividing the power in different proportion. We have also represented the graphical and quantitative aspects of the different types S – Bend optical splitter, depending upon the tilt angle. The analysis represents the numerical analysis with an exact waveguide dimension, which clearly shows the power at various stages of the devices. Depending upon the tilt angle the devices can be categorized into symmetric, asymmetric and highly asymmetric. This discussion clearly indicates that with an increment of the tilt angle the power in the arm decreases, whereas the arm having the less tilt angle contains more amount of the optical power. Here, we are also propose the structures of ≈ 53 nm wavelength tunability. Modal index of all the S-bend structures decreases with respect to the wavelength of the input signal.

ACKNOWLEDGEMENT

The authors would like to acknowledge Opti-Wave 11 for conducting the present research work.

APPENDIX

Analytical Expression for S-Bend Waveguide

In order to perform the analytical analysis of our proposed S-bend power splitter through our proposed BPM discussed in section 3, it is necessary to represent the structural variation of the S-bend structure in analytical form. This section shows the approximate analytical expression of all three types of S-bend structure. It also shows the detailed quantitative comparison for all three S-bend structures. Figure A represents the graphical view of the all three S-bend structure obtained from the actual data points through software and through approximate polynomial form. The value of derived equations for all the S-bend structures is shown in Appendix A.

In order to analyze the appropriateness of our derived approximate polynomial equations, we obtained the error plot between the actual data points and points obtained from interpolated equations. Figure B shows the closeness of the actual S-bend structure with derived equation, as it represents a very small amount of error (%).

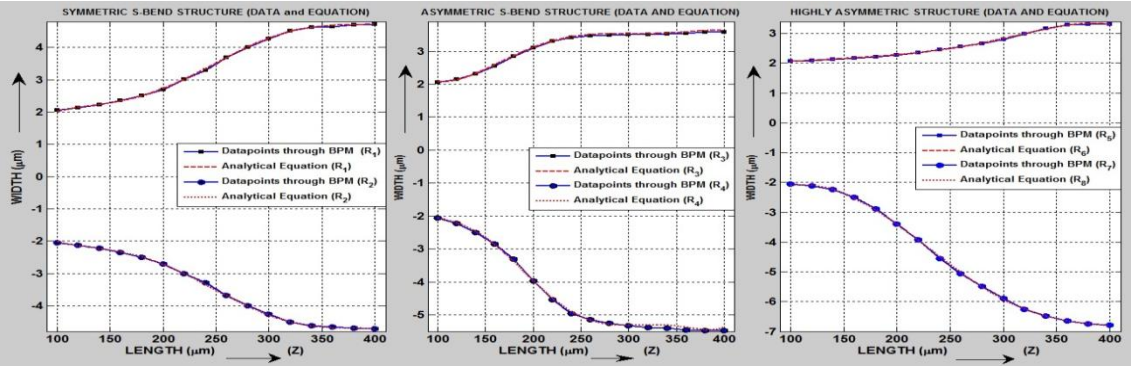

Fig. A: Comparison of all three types of S-bend structures obtained from the actual data points and derived equation.

Hence, this analysis concludes that the derived equation completely defines the actual structure. From this plot % error is very less for symmetric compared to an asymmetric one. Interestingly at midpoint of S-bend structure at ≈ 250 nm, the error is zero for both symmetric/asymmetric waveguide structures as compared to highly asymmetric structure.

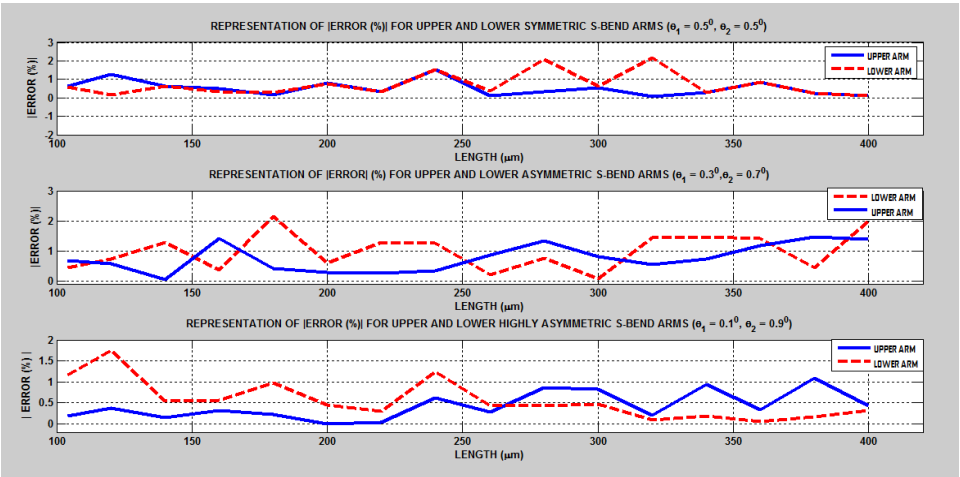

Fig. B: Error (%) plot along the length of the all three types S-bend structure.

Table A: Derived equations for all the S-bend structures.

		Derived Approximate Equation
Symmetric Structure	$R_1(z)$	$z^5 + P_2z^4 + P_3z^3 + P_4z^2 + P_5z + P_6$; where, $P_1 = 1.361 \times 10^{-11}$, $P_2 = -1.721 \times 10^{-8}$, $P_3 = 8.031 \times 10^{-6}$; $P_4 = -0.001698$, $P_5 = 0.1703$, $P_6 = -4.485$
	$R_2(z)$	$P_1z^5 + P_2z^4 + P_3z^3 + P_4z^2 + P_5z + P_6$; where, $P_1 = -1.361 \times 10^{-11}$, $P_2 = 1.721 \times 10^{-8}$, $P_3 = -8.031 \times 10^{-6}$; $P_4 = 0.001698$, $P_5 = -0.1703$, $P_6 = 4.485$
Asymmetric	$R_3(z)$	$P_1z^6 + P_2z^5 + P_3z^4 + P_4z^3 + P_5z^2 + P_6z + P_7$; where,

Structure		$P_1 = -2.157 \times 10^{-14}$, $P_2 = 2.145 \times 10^{-11}$, $P_3 = -4.367 \times 10^{-9}$; $P_4 = -1.979 \times 10^{-6}$, $P_5 = 0.0009674$, $P_6 = -0.1288$, $P_7 = 7.509$
	$R_4(z)$	$P_1z^6 + P_2z^5 + P_3z^4 + P_4z^3 + P_5z^2 + P_6z + P_7$; where, $P_1 = 2.118 \times 10^{-13}$, $P_2 = -3.096 \times 10^{-10}$, $P_3 = 1.779 \times 10^{-7}$; $P_4 = -5.066 \times 10^{-5}$, $P_5 = 0.0007437$, $P_6 = -0.5462$, $P_7 = 13.97$
Highly Asymmetric Structure	$R_5(z)$	$P_1z^5 + P_2z^4 + P_3z^3 + P_4z^2 + P_5z + P_6$; where, $P_1 = -3.623 \times 10^{-12}$, $P_2 = 3.638 \times 10^{-6}$, $P_3 = -1.348 \times 10^{-6}$; $P_4 = 0.002414$, $P_5 = -0.01918$, $P_6 = 2.583$
	$R_6(z)$	$P_1z^5 + P_2z^4 + P_3z^3 + P_4z^2 + P_5z + P_6$; where, $P_1 = -5.762 \times 10^{-12}$, $P_2 = 5.913 \times 10^{-9}$, $P_3 = -1.691 \times 10^{-6}$; $P_4 = -6.0636 \times 10^{-6}$, $P_5 = 0.03632$, $P_6 = -4.515$

Table B: Optical band input signal

Optical Band	Name of Optical Band	Wavelength range
O- Band	Original Band	1260 nm – 1360 nm
E – Band	Extended Band	1360 nm – 1460 nm
S – Band	Short Band	1460 nm – 1530 nm
C – Band	Conventional Band	1530 nm – 1565 nm
L - Band	Long Band	1565 nm – 1625 nm

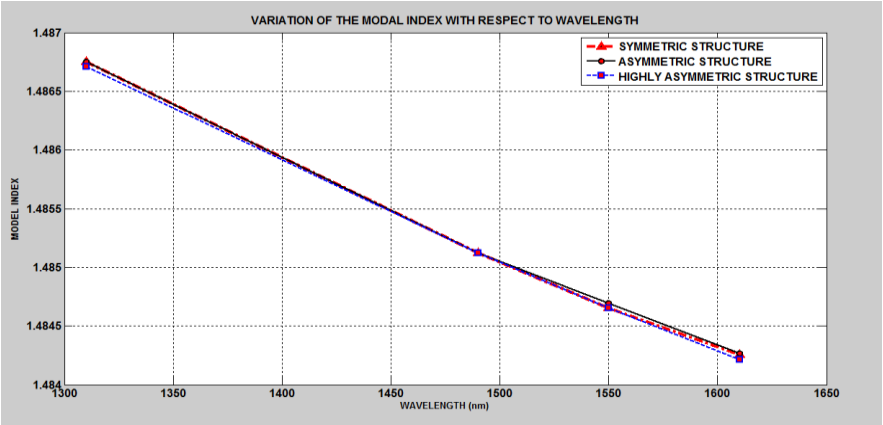

Fig. C: Variations of the modal index/ effective index with respect to wavelengths as at 1330 nm, $n_{eff} = 1.4868$.

REFERENCES

[1] H. Sasaki and N. Mikoshiba, "Normalized power transmission in single mode optical branching waveguide," *Electron. Lett.* **17**(3), 136–138 (1981).

[2] T. D. Ni et. al., "Design, fabrication, and test of wide-angle low-loss Y-junction hybrid polymer couplers," *Appl. Phys. Lett.*, **67**(12), 1651–1652 (1995).

[3] H. B. Lin, R. S. Cheng, and W. S. Wang, "Wide-angle low-loss single mode symmetric Y-junction," *IEEE Photon. Technol. Lett.* **6**(7), 825–827 (1994).

[4] H. Van Brug et. al., "Low-loss straight and curved ridge waveguides in LPE-Grown GalnAsP," *Electro. Lett.* **25**(20), 1330-1332 (1989).

[5] F. J. Mustieles, E. Ballesteros, and P. Baquero, "Theoretical S-bend profile for optimization of optical waveguide radiation losses," *IEEE Photon. Technol. Lett.* **5**(5), 551-553 (1993).

[6] Anuj Bhatnagar, "Study of cross coupling in transition bends using cascaded coupler segment method," *IEEE Photon. Technol. Lett.* **6**(8), 1004-1007 (1994).

[7] Y. Tsuji and M. Koshiba, "A finite element beam propagation method for strongly guiding and longitudinally varying optical waveguides," *J. Lightw. Technol.* **14**(2), 217-222 (1996).

[8] M. D. Feit and J. A. Fleck, Jr., "Light propagation in graded index optical fibers," *Appl. Opt.* **17**(24), 3990-3998 (1978).
[9] L. Thylen and D. Yevick, "Beam propagation method in anisotropic media," *Appl. Opt.* **21**(15), 2751-2754 (1982).
[10] D. Yevick and B. Hermansson, "New formulations of the matrix beam propagation method: Application to rib waveguides," *IEEE J. Quantum Electron.* **25**(2), 221-229 (1989).
[11] Ella V. Bekker et. al., Wide-angle alternating-direction implicit finite-difference beam propagation method," *J. Lightw. Technol.* **27**(14), 2595-2604 (2009).
[12] Haifeng Zhou et. al, "Analysis of an MMI-based six-port circulator by using 3-d magneto-optical beam propagation method," *J. Lightw. Technol.* **27**(21), 4660-4666 (2009).
[13] Sami A. Shakir, Raymond Andrew Motes, and Richard W. Berdine, "Efficient scalar beam propagation method," *IEEE J. Quant. Electron*., **47**(4) 2011.
[14] R. Andrew Motes, Sami A. Shakir, and Richard W. Berdine, "An efficient scalar, non-paraxial beam propagation method," *J. Lightw. Technol.* **30**(1), 4-8 (2012).
[15] Zhen Hu and Ya Yan Lu, "Computing optimal waveguide bends with constant width," *J. Lightw. Technol.* **25**(10), 3161-3167 (2007).
[16] Y. Y. Lu and P. L. Ho, "Beam propagation modeling of arbitrarily bent waveguides," *IEEE Photon. Technol. Lett.*, **14**(12), 1698–1700 (2002).
[17] C. Chaudhari, D. S. Patil, D. K. Gautam, "A new technique for the reduction of the power loss in the Y-branch optical power splitter," *Opti. Comm.* **193**, 121-125 (2001).
[18] H. F. Taylor, "Power loss at directional change in dielectric waveguides," *Appl. Opt.* **13**(3), 642–647 (1974).
[19] Chih-Wei Hsu, Hsuen-Li Chen, and Way-Seen Wang, "Compact Y -branch power splitter based on simplified coherent coupling," *IEEE Photon. Technol. Lett.* **15**(8), 1103-1105 (2003).
[20] Xiaoqing Jiang et. al., "Low crosstalk 1×2 thermooptic digital optical switch with integrated S-bend attenuator," *IEEE Photon. Technol. Lett.* **18**(4), 610-612 (2006).
[21] M. E. Solmaz et. al., "Compact bends for achieving higher integration densities for $LiNbO_3$ waveguides," *IEEE Photon. Technol. Lett.* **21**(9), 557-579 (2009).
[22] S. Tao et. al., "An optical power splitter with variable power splitting ratio," *IEEE Photon. Technol. Lett.* **23**(14), 1004-1006 (2011).
[23] P. P. Sahu, "A double S-bend geometry with lateral offset for compact two mode interference coupler," *J. Lightw. Technol.* **29**(13), 2064-2068 (2011).
[24] S. K. Raghuwanshi, S. Kumar, V. Kumar, and D. Chack, "Propagation study of Y-branch having inbuilt optical splitters and combiner using beam propagation method," *Progress In Electromagnetics Research Symposium Proceedings*, pp. 720-724, Moscow, Russia, August 19-23, 2012.
[25] John P. George, N. Dasgupta, and B.K. Das, "Compact integrated optical directional coupler with large cross section silicon waveguides," *Proc. SPIE* **7719**, 77191X (2010).
[26] Zhao et. al., "Ultracompact and large-scale power splitters on silicon-based two-dimensional photonic crystals at near-infrared wavelengths," *Optical Engineering* 45(02), (2006).
[27] Wei Li et. al., "An ultra-short 1×2 double-wavelength optical power splitter for 1310/1550-nm operation based on photonic crystal multimode interference," *Proc. SPIE* **7631**, 76312J (2009).
[28] R. K. Navalakhe, N. D. Gupta, and B. K. Das, "Fabrication and Characterization of Straight and Compact S-bend Optical Waveguides on a Silicon-on-Insulator Platform," *Appl. Opt*., **48** (31), G125-G130 (2009).
[29] Shyh-Lin Tsao and Chun-Yi Lu, "BPM simulation and comparison of 1×2 directional waveguide coupling and y-junction coupling silicon-on-insulator optical couplers," *Fiber and Integrated Optics*, **21**, 417–433 (2002).
[30] Tzyy-Jiann Wang, Chih-Feng Huang, and Way-Seen Wang, "Wide-Angle Optical Power Divider in $LiNbO_3$ for Variable Power Splitting," *IEEE Phot. Technol. Lett.* **15**(10), 1401-1403 (2003).
[31] Yinian Zhu, Chao Lu, B.M. Lacquet, P.L. Swart, S.J. Spammer, "Wavelength-tunable add/drop multiplexer for dense wavelength division multiplexing using long-period gratings and fiber stretchers," *Opti. Commun.* **208**, 337–344, (2002).
[32] K. T. Kim, J. W. Song, "Investigation of thermo-optically tunable fiber-to-planar waveguide coupler," *Opti. Commun*. **205**, 113–121, (2002).
[33] Y. Chung and N. Dagli, "An assessment of finite difference beam propagation method," *IEEE J. Quant. Electron.* **26**(8), 1335-1339 (1990).
[34] J. Yamauchi, J. Shibayama, and H. Nakano, "Modified finite difference beam propagation method on the generalized Douglas scheme for variable coefficients," *IEEE Photon. Technol. Lett*., **7**(6), 661-663 (1995).
[35] Y. Tsuji and M. Koshiba, "Afinite beam propagation method for strongly guiding and longitudinally varying optical waveguides," *J. Lightw. Technol.* **14**(2), 217-222 (1996).
[36] K. Kawano, and T. Kitoh, "Introduction to optical waveguide analysis," A willey-Interscience Publication, Chapter 5 (2001).
[37] S. K. Raghuwanshi and S. Talabattula, "Analytical approximation solutions for 3-D optical waveguides: Review," *Indian J. Phys.* **83(**2), 127-151 (2009).